

MIT Open Access Articles

Loss of a satellite could explain Saturn's obliquity and young rings

The MIT Faculty has made this article openly available. **Please share** how this access benefits you. Your story matters.

Citation: Wisdom, Jack, Dbouk, Rola, Militzer, Burkhard, Hubbard, William B, Nimmo, Francis et al. 2022. "Loss of a satellite could explain Saturn's obliquity and young rings." Science, 377 [6612].

As Published: 10.1126/SCIENCE.ABN1234

Publisher: American Association for the Advancement of Science (AAAS)

Persistent URL: <https://hdl.handle.net/1721.1/148216>

Version: Author's final manuscript: final author's manuscript post peer review, without publisher's formatting or copy editing

Terms of use: Creative Commons Attribution-Noncommercial-Share Alike



Loss of a Satellite Could Explain Saturn's Obliquity and Young Rings

Jack Wisdom,^{1*} Rola Dbouk,¹ Burkhard Militzer,² William B. Hubbard,³
Francis Nimmo,⁴ Brynna G. Downey⁴, Richard G. French⁵

¹Massachusetts Institute of Technology, Cambridge, MA 02139, USA

²University of California, Berkeley, CA 94720 USA

³University of Arizona, Tucson, AZ 85721-0092, USA

⁴University of California, Santa Cruz, CA 95064, USA

⁵Wellesley College, Wellesley, MA 02481, USA

*To whom correspondence should be addressed; E-mail: wisdom@mit.edu.

The origin of Saturn's $\sim 26.7^\circ$ obliquity and ~ 100 Myr old rings is unknown. The observed rapid outward migration of Saturn's largest satellite, Titan, could have raised Saturn's obliquity through a spin-orbit precession resonance with Neptune. We use Cassini data to refine estimates of Saturn's moment of inertia, finding that it is just outside the range required for the resonance. We propose that Saturn previously had an additional satellite, which we name Chrysalis, that caused Saturn's obliquity to increase through the Neptune resonance. Destabilization of Chrysalis's orbit ~ 100 Myr ago can then explain the proximity of the system to the resonance and the formation of the rings through a grazing encounter with Saturn.

Saturn's obliquity, the angle between its equator and the plane of its orbit around the Sun, is too large to have arisen during Saturn's formation from a protoplanetary disk, or from a large

impact (1). Saturn's rings appear to be only ~ 100 Myr old, based on the estimated strength of satellite ring torques (2) and the estimated rate of darkening of the ice-rich material (3, 4). However, the lack of a suitable mechanism to explain such young rings has led some to question the young age (5).

The precession frequency of Saturn's spin axis (the rate at which the axis rotates about the vertical) is close to the precession frequency of Neptune's orbit (6). This raises the possibility that the obliquity resulted from a resonance between these two frequencies. Resonances between the precession of the spin axis of a body and the precession of its orbit occur elsewhere in the Solar System. The spin axis of the Moon and the orbit of the Moon precess at the same rate (7, 8). Spin-orbit precession resonances also arise if the precession frequency of a spin axis is close to a frequency component in the precession of its orbit. Mars has a chaotic obliquity due to a resonance between the precession of its spin axis and a chaotically varying component in its orbit precession associated with the precession of Venus (9, 10). The obliquity of the Moon, locked in the precession resonance, depends on the rate of mutual precession of the orbit and spin axis. The Moon's obliquity was different in the past because the rate of orbit precession depends on the distance to the Earth, and the Moon is tidally evolving outward from the Earth. There were times when the obliquity of the Moon was large (11).

If the large obliquity of Saturn is the result of a spin-orbit resonance between the precession of Saturn's spin axis and the precession of the orbit of Neptune, how would this have come about? One proposal is that the precession frequency of Neptune's orbit could have changed as the distribution of protoplanetary mass changed during planet formation (1). An alternative proposal relies upon the observed rapid migration of Saturn's largest satellite, Titan (12–14). The precession frequency of Saturn is modified by the presence of its satellites, which are locked to orbit in the equatorial plane of Saturn. Because of this lock, the Sun's gravitational pull on the satellites contributes to the torque that precesses Saturn. The precession of Saturn is dominated

by these solar torques on Titan, which are proportional to the square of the distance of Titan from Saturn (11), so as Titan migrates outwards the precession frequency increases. This could have caused the precession frequency of the Saturn system to become resonant with the precession of Neptune (12). We define a resonance angle σ to be the longitude of Saturn’s equator minus the longitude of the descending node of Neptune’s orbit (10). While in the Neptune resonance this angle oscillates about zero. If the migration of Titan was slow, compared to the period of oscillation in the precession resonance, the obliquity of Saturn could have risen as Titan migrated (13).

Both of these scenarios require the moment of inertia of Saturn to be in a certain range, and predict that the system is currently in this spin-orbit precession resonance. Previous determinations of the moment of inertia had too high an uncertainty to draw definitive conclusions (1, 12).

Moment of inertia of Saturn The exterior gravity field of Saturn, as determined using the Cassini spacecraft (4), provides tight constraints on models of the planet’s interior structure. We constructed interior models using four different sets of assumptions. For a range of rotation periods, the corresponding moments of inertia are shown in Fig. 1 in terms of the normalized angular momentum: the product of the moment of inertia and the rotation rate, normalized by $MR_e^2\sqrt{GM/R_e^3}$, where G is the gravitational constant, M is the mass of Saturn, and R_e is its fiducial equatorial radius, taken to be 60268 km (15).

We combine an equation of state (EOS) for hydrogen-helium mixtures (16) with assumptions about Saturn’s interior composition. We assume the interior of Saturn is differentially rotating on cylinders, chosen to match cloud tracking observations. We employ the concentric Maclaurin spheroid (CMS) method (17, 18) to construct models that match (Fig. S1) the gravitational moments from J_2 to J_{12} (4). The J s are dimensionless coefficients in the expansion of the exterior gravity field. Normalized angular momentum values are shown in Fig. 1 and listed

in Table S1.

To estimate how much the computed moment of inertia depends on the assumptions, we employed three additional approaches to construct models of the interior of Saturn. These models only match the gravitational moments J_2 , J_4 , and J_6 without invoking differential rotation.

The first approach uses the consistent level curve (CLC) method (19), with polynomial EOSs that relate pressure and density. The order of the polynomial is increased until the values of J_2 to J_6 can be reproduced. The second approach uses the CMS method as before, but introduces a single discontinuity in the density to match J_2 to J_6 without differential rotation. The third method introduces more flexibility by representing Saturn’s interior with four constant-density spheroids. Their densities and thicknesses are adjusted until the observed moments up to J_6 can be matched with CMS calculations. The resulting spread of model predictions is indicated in Fig. 1 and Fig. S2. Results for a larger number of spheroids are shown in Fig. S3. We find consistent results from all models that match J_2 , J_4 , and J_6 while assuming uniform rotation. The angular momentum depends only on the assumed rotation rate and the observed gravitational moments.

Models that assume uniform rotation do not match the high-order gravitational moments (J_8 - J_{12}). The observed large magnitudes of the high-order moments is indicative of differential rotation (4, 20). However, the inclusion of differential rotation lowers the implied angular momentum by only $\sim 0.5\%$ (Fig. 1).

The resulting moments of inertia are in close agreement with one another, indicating that they are tightly constrained by the gravitational moments and insensitive to the assumed composition and equation of state. The values of J_2 and J_4 alone provide sufficient constraints on the planet’s angular momentum to show that Saturn is slightly out of resonance with Neptune (see Supplementary Text). Models without differential rotation provide an upper bound on the angular momentum, while including differential rotation (to match the higher-order gravitational

moments) reduces the angular momentum slightly (Fig. 1 and Fig. S4) (see Supplementary Text).

Numerical integrations of the satellite system We used numerical integration to investigate the dynamical evolution of the Saturn satellite system. These integrations include Saturn, modelled as a rigid body, the gravitational moments of Saturn from J_2 to J_6 , the major satellites of Saturn from Mimas to Iapetus, the Sun, and the other three outer planets. The system is fully coupled: the gravitational moments affect the motion of the satellites as well as the rotation of Saturn. Some of our integrations included tidal evolution, specified by the rate of change of Titan’s semimajor axis; for simplicity we ignore the tidal evolution of the other satellites (21).

We used direct numerical integration to determine the range of moments of inertia of Saturn for which the system is in the spin-orbit precession resonance. Numerical integration avoids the need to analytically estimate a host of small effects (21). We refer to the lower bound of this range as the critical value. We performed a series of forward and backward 50 Myr integrations to determine the critical moment of inertia. These integrations did not include tidal friction and excluded the tiny satellite Hyperion. The results are also shown in Fig. 1, in terms of the normalized angular momentum. We find that the system is outside, but close to, the resonance region for all model assumptions and rotation periods. If we adopt a rotation period of 10:33:34 h, derived by matching Saturn’s flattening (15, 18), the predicted angular momenta are between 0.5% and 1.0% below the critical value.

The critical angular momentum to be in resonance corresponds to a dimensionless polar moment of inertia of 0.2201. The estimated value, with differential rotation, for a rotation period of 10:33:34 h is $0.2182^{+0.0006}_{-0.0003}$, which is about 1% below the critical value. Previous work (12), though more approximate, found that for Saturn to have had an initial obliquity less than 10° the moment of inertia must be in the range 0.224 to 0.237, and to be oscillating in the

resonance it must be between 0.22 and 0.24, a 10% range.

Small changes in the system parameters can make large changes in the rate of precession. For example, changing the semimajor axis of Saturn by only 5% changes the rate of precession by 15% (Eq. 1 below). Similarly, making small changes in the mass or position of Uranus or Neptune can also make large changes in the precession frequency of Neptune. So the system being only 1.0% away from the resonance suggests that the Neptune resonance has played a role in the recent history of the Saturn system.

The rapid migration of Titan rules out scenarios that depend on the Neptune resonance in the early Solar System (12). If the Neptune resonance played a role in the development of the obliquity of Saturn, it rules out other proposed early Solar System explanations (22, 23). We propose that the obliquity of Saturn arose because the system was previously trapped in the Neptune resonance as Titan migrated outwards, but escaped from the resonance recently enough to still be near the resonance.

Resonance model We construct a simple model that captures many aspects of the dynamics of the spin-orbit precession resonance with Neptune (21). This model can be used to interpret the results of the full numerical simulations.

A parameter in this model is the precession constant. Averaging over the orbital timescale, an oblate planet with satellites orbiting the Sun in a fixed circular orbit has a rate of regression of the spin axis of $\alpha \cos(\epsilon)$ where α is the precession constant and ϵ is the obliquity of the spin axis to the fixed orbit normal. The precession constant is (11, 13)

$$\alpha = \frac{3}{2} n \frac{J_2 + q}{\omega \lambda + l}, \quad (1)$$

where n is the orbital frequency, ω is the rotation rate, J_2 is the second gravitational moment, and $\lambda = C/(MR_e^2)$, the dimensionless polar moment of inertia, and

$$\begin{aligned}
q &= \frac{1}{2} \sum_j \frac{m_j}{M} \frac{a_j^2}{R_e^2} \frac{\sin(2(\epsilon - i_j^L))}{\sin(2\epsilon)} \\
l &= \sum_j \frac{m_j}{M} \frac{a_j^2}{R_e^2} \frac{n_j}{\omega} \frac{\sin(\epsilon - i_j^L)}{\sin(\epsilon)},
\end{aligned} \tag{2}$$

The sum is over all the satellites, m_j is the mass of the satellite, a_j is the semimajor axis of the satellite, n_j is its orbital frequency. The angle i_j^L is the inclination of the Laplace plane to the planetary equator (24); the normal to the Laplace plane is the direction about which the normal to the satellite orbit precesses. For a close satellite the Laplace plane coincides with the planetary equator plane, while for a distant satellite it coincides with the plane of the orbit of the planet about the Sun. The magnitude of i_j^L depends on the planetary oblateness and obliquity, and the semimajor axes involved.

Eq. (2) shows that the contribution from each satellite to q , the factor that is added to J_2 , is proportional to the product of the mass of the satellite and the square of its distance from the planet. The contribution of Titan to the precession constant dominates the contribution from J_2 , and this contribution increases as Titan migrates outwards.

Resonance escape mechanisms We next consider how the Saturn system could have escaped the resonance with Neptune. We identify two possibilities: First, the satellites' contribution to the precession of Saturn could have changed due to changes in their orbits (Eq. 2). This might have happened by the passage of the system through an orbital resonance involving the satellites. Second, the system could have escaped the Neptune resonance if a satellite was ejected from the system or collided with Saturn (removing a term in the sum in Eq. 2). A close encounter of a satellite with Saturn could have produced the debris that has evolved into the rings.

We investigated the first possibility through direct integration of the system using the full numerical model. We find that two principal orbital resonances are encountered (see Supple-

mentary Text), which have been previously studied (25, 26). We have carried out integrations of the full system backward in time for ~ 200 Myr, with Saturn moments of inertia that were determined with differential rotation, and with various rates of tidal evolution that are consistent with the measured rate of evolution of Titan (21). These integrations confirm that the Saturn system is currently not in the Neptune resonance.

In no case did we find changes in the satellite orbits that were sufficiently large to allow the system to escape the Neptune resonance. Fig. 2 shows an example numerical integration. The evolution coincides with the resonance model over the full span of the integration, indicating that passage through these orbital resonances cannot take the system out of the Neptune resonance. The comparison also illustrates that no other, previously unknown, strong orbital resonance was encountered.

Instability of an additional satellite The second possibility is that there was previously an additional satellite in the Saturn system, and that this satellite suffered some orbital instability that either led to its escape or collision with Saturn. With the loss of the hypothetical satellite, Chrysalis, the precession rate would have suddenly changed, allowing the system to escape the Neptune resonance. By requiring that the system evolved to the present configuration, we place constraints on when this could have occurred.

While in the Neptune resonance the resonance angle σ oscillates about zero. Because σ does not change when a satellite is lost, Chrysalis could only have been lost when σ was close to zero in the simulations of the full system, backward in time from the present, without Chrysalis.

We have determined that the moment of inertia of Saturn is a little too small for the system to be in the Neptune resonance today, or the precession constant is a little too high. In the past, as Titan was closer to Saturn, the precession constant was smaller (Eq. 2). Therefore, there was a moment in the past at which the system crossed the resonance. Fig. 2 shows this

happens in the example simulation at about 100 Myr before present, where the motion of σ reverses direction. Fig. 3 shows the evolution in terms of the precession constant. The loss of Chrysalis connects the evolution with Chrysalis to the evolution without Chrysalis. The system evolves into the resonance, then to higher obliquity as the precession constant changes due to the migration of Titan, at which point Chrysalis could have been lost, causing the precession constant to suddenly decrease. The subsequent evolution passes through the resonance to the currently observed Saturn system.

In this example simulation, the most recent time that Chrysalis could have been lost is about 160 Myr before present. In the full suite of simulations that vary the rate of tidal evolution of Titan, we find that the loss of Chrysalis could have occurred roughly 100-200 Myr before present. The combination of evolution in the Neptune resonance, followed by recent loss of Chrysalis, accounts for both the present-day obliquity of Saturn and the system's proximity to the Neptune resonance.

To explore the possibility that Chrysalis's orbit was destabilized, we integrated the full system with Chrysalis placed between Titan and Iapetus. As Titan migrates in the simulations, the Titan-Chrysalis pair encounters orbital resonances. We focused our exploration on the 3:1 mean-motion resonance (at which the orbital period of Chrysalis is approximately three times the orbital period of Titan), because this is the first strong resonance that would have been encountered as Titan migrated outwards. The mass of Chrysalis must be chosen so that the precession constant has the required change. For the 3:1 resonance the mass of Chrysalis must be approximately the mass of Iapetus, though the value depends on when the 3:1 resonance is encountered, which in turn depends on the rate of tidal evolution of Titan. In these simulations, we set the tidal evolution rate for Titan to be 13.75 cm yr^{-1} , and the mass of Chrysalis to equal the mass of Iapetus. The initial conditions are taken from the backward simulation shown in Fig. 2.

We carried out integrations with Titan’s orbital semimajor axis initially smaller than required to be in the 3:1 resonance with Chrysalis. As Titan migrates outward, the system reaches the resonance, the behavior becomes chaotic, and the orbital eccentricity of Chrysalis rapidly increases, leading to close encounters with the other satellites (Fig. S5).

Exploration of an unstable system We explored the expected outcomes of this scenario by simulating the system starting in the chaotic zone of the 3:1 Titan-Chrysalis resonance. We studied 390 cases, started with slightly different initial conditions (21). These integrations included Hyperion, because Chrysalis repeatedly crosses its orbit. The present obliquity of Saturn could be explained if Chrysalis was either lost by ejection on a hyperbolic orbit, or by being broken up during a grazing encounter with Saturn, with most of the material eventually hitting Saturn. In the latter case, a breakup of the satellite could explain the age of the Saturn’s rings.

The evolution of Chrysalis follows a typical pattern. In the first stage the eccentricity and semimajor axis explore the chaotic zone and migrate to larger eccentricity. This stage is illustrated for an example simulation in Fig. 4A. This is followed by numerous close encounters with both Titan and Iapetus. The number of encounters varies, but is typically of order a few tens. These encounters lead to an increase in the semimajor axis and eccentricity of Chrysalis. This stage is illustrated in Fig. 4B. Eventually, Chrysalis either has a close encounter with Saturn, is ejected from the satellite system, or has a collision with Titan, Hyperion, or Iapetus. For the simulation in Fig. 4, Chrysalis has a grazing encounter with Saturn at a distance of $1.9R_e$, close enough to undergo tidal disruption followed by formation of a ring (27).

Of our 390 simulations, there were 90 cases in which Hyperion was left with an orbit that was within $1.5R_e$ of its present orbit. Of these there were 19 cases in which Chrysalis became hyperbolic (21%), and 17 Saturn grazers (18%) (the distance became smaller than $2.5R_e$ from Saturn, see Supplementary Text). Both of these cases would allow the system to escape the

Neptune resonance (39%); those with Saturn grazers could make the rings. Hyperion's orbit is modified somewhat, so we cannot determine where it originated before Chrysalis was scattered. In 8 of the 17 grazing cases (47%) Hyperion was left librating in the Titan-Hyperion 4:3 mean motion resonance, as observed today (28).

The simulated Chrysalis has multiple encounters with Titan and Iapetus, so we expect that their orbits were modified. Titan's orbital eccentricity is of particular interest, as its relatively large value of 0.0288 has been considered a puzzle (29). In these integrations, we set the initial eccentricity of Titan to be zero; at the time of the encounter of Chrysalis with Saturn, we find that the eccentricity of Titan ranges from 0.004 to 0.055, with a mean of 0.026 and standard deviation of 0.015 (Fig. 5). The scattering of Chrysalis off of Titan leads to an orbital eccentricity of Titan similar to the current value.

We conclude that the loss of the hypothetical satellite Chrysalis can explain the obliquity of Saturn, the young age of its rings, and the eccentricity of Titan. The increased eccentricity and concomitant tidal heating (proportional to the square of the eccentricity) of Titan might also explain the presence of short-lived methane in its atmosphere (30).

Formation of Saturn's rings A close encounter of Chrysalis with Saturn would have caused Chrysalis to break apart. If we assume Chrysalis was predominantly made of water ice, like Iapetus, then this debris could have developed into Saturn's rings (27). Previous simulations of the formation of the rings from a disrupted cometary body, similar to the mass we assume for Chrysalis, indicate that it provides enough to produce the present-day rings (31).

The required timing of the loss of Chrysalis coincides with the estimated age of the rings. In our scenario, the ring age is anchored to a measured quantity, the rate of Titan's orbital expansion (14).

We propose that Saturn once had an additional satellite, Chrysalis, that the system was pre-

viously in the spin-orbit precession resonance with Neptune, that Saturn's obliquity increased as the precession rate changed due to the migration of Titan, that it escaped the precession resonance because of an instability of the orbit of Chrysalis, and that a close encounter of this hypothesized satellite with Saturn led to the formation of its rings.

References

1. W. R. Ward, D. P. Hamilton, Tilting Saturn. I. Analytic Model. *Astrophysical Journal* **128**, 2501-2509 (2004).
2. P. Goldreich, S. Tremaine, The dynamics of planetary rings. *Ann. Rev. Astron. Astrophys.* **20**, 249-283 (1982).
3. Z. Zhang, *et al.*, Exposure age of Saturn's A and B rings, and the Cassini Division as suggested by their non-icy material content. *Icarus* **294**, 14-42 (2017).
4. L. Iess, *et al.*, Measurement and implications of Saturn's gravity field and ring mass. *Science* **364**, aat2965 (2019).
5. A. Crida, S. Charnoz, H.-W. Hsu, L. Dones, Are Saturn's rings actually young? *Nature Astronomy* **3**, 967-970 (2019).
6. A. W. Harris, W. R. Ward, Dynamical Constraints on the Formation and Evolution of Planetary Bodies. *Annual Review of Earth and Planetary Sciences* **10**, 61 (1982).
7. G. Cassini, *Traite de L'origine ede Progres de L'Astronomie* (Paris, 1693).
8. S. J. Peale, Generalized Cassini's Laws. *Astronomical Journal* **74**, 483 (1969).
9. J. Laskar, P. Robutel, The chaotic obliquity of the planets. *Nature* **361**, 608-612 (1993).

10. J. Touma, J. Wisdom, The Chaotic Obliquity of Mars. *Science* **259**, 1294-1297 (1993).
11. W. R. Ward, Past Orientation of the Lunar Spin Axis. *Science* **189**, 377-379 (1975).
12. M. Saillenfest, G. Lari, G. Boué, The large obliquity of Saturn explained by the fast migration of Titan. *Nature Astronomy* **5**, 345-349 (2021).
13. M. Saillenfest, G. Lari, G. Boué, A. Courtot, The past and future obliquity of Saturn as Titan migrates. *Astronomy and Astrophysics* **647**, A92 (2021).
14. V. Lainey, *et al.*, Resonance locking in giant planets indicated by the rapid orbital expansion of Titan. *Nature Astronomy* **4**, 1053-1058 (2020).
15. G. F. Lindal, D. N. Sweetnam, V. R. Eshleman, The atmosphere of Saturn - an analysis of the Voyager radio occultation measurements. *Astronomical Journal* **90**, 1136-1146 (1985).
16. B. Militzer, W. B. Hubbard, Ab Initio Equation of State for Hydrogen-Helium Mixtures with Recalibration of the Giant-planet Mass-Radius Relation. *Astrophys. J.* **774**, 148 (2013).
17. W. B. Hubbard, Concentric Maclaurin Spheroid Models of Rotating Liquid Planets. *Astrophysical Journal* **768**, 43 (2013).
18. B. Militzer, S. Wahl, W. B. Hubbard, Models of Saturn's Interior Constructed with an Accelerated Concentric Maclaurin Spheroid Method. *Astrophysical Journal* **879**, 78 (2019).
19. J. Wisdom, W. B. Hubbard, Differential rotation in Jupiter: A comparison of methods. *Icarus* **267**, 315-322 (2016).
20. W. B. Hubbard, Gravitational Signature of Jupiter's Deep Zonal Flows. *Icarus* **137**, 357-359 (1999).

21. Materials and methods are provided in the supplementary materials.
22. S. Tremaine, On the origin of the obliquities of the outer planets. *Icarus* **89**, 85-92 (1991).
23. R. Brasser, M. H. Lee, Tilting Saturn without Tilting Jupiter: Constraints on Giant Planet Migration. *Astronomical Journal* **150**, 157 (2015).
24. S. Tremaine, J. Touma, F. Namouni, Satellite Dynamics on the Laplace Surface. *Astronomical Journal* **137**, 3706-3717 (2009).
25. W. Polcarpe, M. Saillenfest, V. Lainey, A. Vienne, B. Noyelles, N. Rambaux, Strong tidal energy dissipation in Saturn at Titan's frequency as an explanation for Iapetus orbit. *Astronomy and Astrophysics* **619**, A133 (2018).
26. M. Čuk, L. Dones, D. Nesvorný, K. J. Walsh, Secular resonance between Iapetus and the giant planets. *Mon. Not. R. Astron. Soc.* **481**, 5411-5421 (2018).
27. L. Dones, A recent cometary origin for Saturn's rings? *Icarus* **92**, 194-203 (1991).
28. A. T. Sinclair, On the origin of the commensurabilities amongst the satellites of saturn. *Monthly Notices of the Royal Astronomical Society* **160**, 169–187 (1972).
29. C. Sagan, S. F. Dermott, The tide in the seas of Titan. *Nature* **300**, 731-733 (1982).
30. G. Tobie, J. I. Lunine, C. Sotin, Episodic outgassing as the origin of atmospheric methane on Titan. *Nature* **440**, 61-64 (2006).
31. R. Hyodo, S. Charnoz, K. Ohtsuki, H. Genda, Ring formation around giant planets by tidal disruption of a single passing large Kuiper belt object. *Icarus* **282**, 195-213 (2017).
32. J. Wisdom *et al.* SaturnObliquityRings, Harvard Dataverse Repository (2022); <https://doi.org/10.7910/DVN/RJZXGW>.

33. J. Wisdom, NbodySatellites, Zenodo (2022); <https://doi.org/10.5281/zenodo.6960630>.
34. Jet Propulsion Laboratory, California Institute of Technology, NAIF, Planetary Data System Navigation Node: *ftp://ssd.jpl.nasa.gov/pub/eph/planets/bsp/de440.bsp*.
35. Jet Propulsion Laboratory, California Institute of Technology, NAIF, Planetary Data System Navigation Node: *ftp://ssd.jpl.nasa.gov/pub/eph/satellites/bsp/sat440l.bsp*.
36. J. Wisdom, M. Holman, Symplectic maps for the N-body problem. *Astronomical Journal* **102**, 1528-1538 (1991).
37. J. Touma, J. Wisdom, Lie-Poisson Integrators for Rigid Body Dynamics in the Solar System. *Astronomical Journal* **107**, 1189 (1994).
38. J. Wisdom, M. Holman, J. Touma, Symplectic Correctors. *Fields Institute Communications* **10**, 217 (1996).
39. J. Wisdom, D. M. Hernandez, A fast and accurate universal Kepler solver without Stumpff series. *MNRAS* **453**, 3015-3023 (2015).
40. G.J.Sussman, J.Wisdom, *Structure and Interpretation of Classical Mechanics* (MIT Press, 2001, 2nd edition, 2014).
41. R. G. French, *et al.*, Noncircular features in Saturn's rings IV: Absolute radius scale and Saturn's pole direction. *Icarus* **290**, 14-45 (2017).
42. J. Wisdom, Dynamics of the Lunar Spin Axis. *Astronomical Journal* **131**, 1864-1871 (2006).
43. J. H. Applegate, M. R. Douglas, Y. Gursel, G. J. Sussman, J. Wisdom, The outer solar system for 200 million years. *Astronomical Journal* **92**, 176-194 (1986).

44. J. Fuller, J. Luan, E. Quataert, Resonance locking as the source of rapid tidal migration in the Jupiter and Saturn moon systems. *Mon. Not. R. Astron. Soc.* **458**, 3867-3879 (2016).
45. W. M. Kaula, Tidal Dissipation by Solid Friction and the Resulting Orbital Evolution. *Reviews of Geophysics and Space Physics* **2**, 661-685 (1964).
46. D. Durante, D. J. Hemingway, P. Racioppa, L. Iess, D. J. Stevenson, Titan’s gravity field and interior structure after Cassini. *Icarus* **326**, 123-132 (2019).
47. B. G. Downey, F. Nimmo, I. Matsuyama, Inclination damping on Callisto. *Mon. Not. R. Astron. Soc.* **499**, 40-51 (2020).
48. W. Polycarpe, V. Lainey, A. Vienne, B. Noyelles, M. Saillenfest, N. Rambaux, *AAS/Division of Dynamical Astronomy Meeting* (2018), vol. 49 of *AAS/Division of Dynamical Astronomy Meeting*, p. 9.
49. E. Roche, Académie des sciences et lettres de montpellier. *Mém. Sect. Sci* **1**, 243–262 (1847).
50. S. Sridhar, S. Tremaine, Tidal disruption of viscous bodies. *Icarus* **95**, 86-99 (1992).
51. A. R. Dobrovolskis, Tidal disruption of solid bodies. *Icarus* **88**, 24-38 (1990).

Acknowledgments

We thank J. Touma, S. Tremaine, and T. Perron for carefully reading the manuscript. C. Hill provided computing time on the MIT Engaging Cluster. **Funding:** Support for this work was provided by NASA’s SSW program (J.W., F.N., and R.D.), NASA’s extended Juno mission (W.H. and B.M.), NNSA (B.M.), NASA’s CDAP program (R.F.), and the NSF GRFP (B.D.). **Author contributions:** J.W. and F.N. designed the overall research, J.W. noticed that Titan’s

migration could lead to capture in the Neptune resonance, B.M., W.H., and J.W. developed interior models, J.W. wrote the satellite evolution software, R.D. developed the resonance model, J.W. suggested that an extra satellite might have been resonantly destabilized and form the rings, R.D. identified the conditions for escape, J.W. and R.D. carried out the simulations and analysis. F.N. and B.D. provided input throughout. R.F. validated the numerical model of Saturn's pole. **Competing interests:** The authors declare no competing interests. **Data and Materials:** All data and software have been deposited in Harvard Dataverse (32). The satellite evolution code is also available on Zenodo (33).

Supplementary materials

Materials and Methods

Supplementary Text

Figs. S1-S5

Table S1

References (34-51)

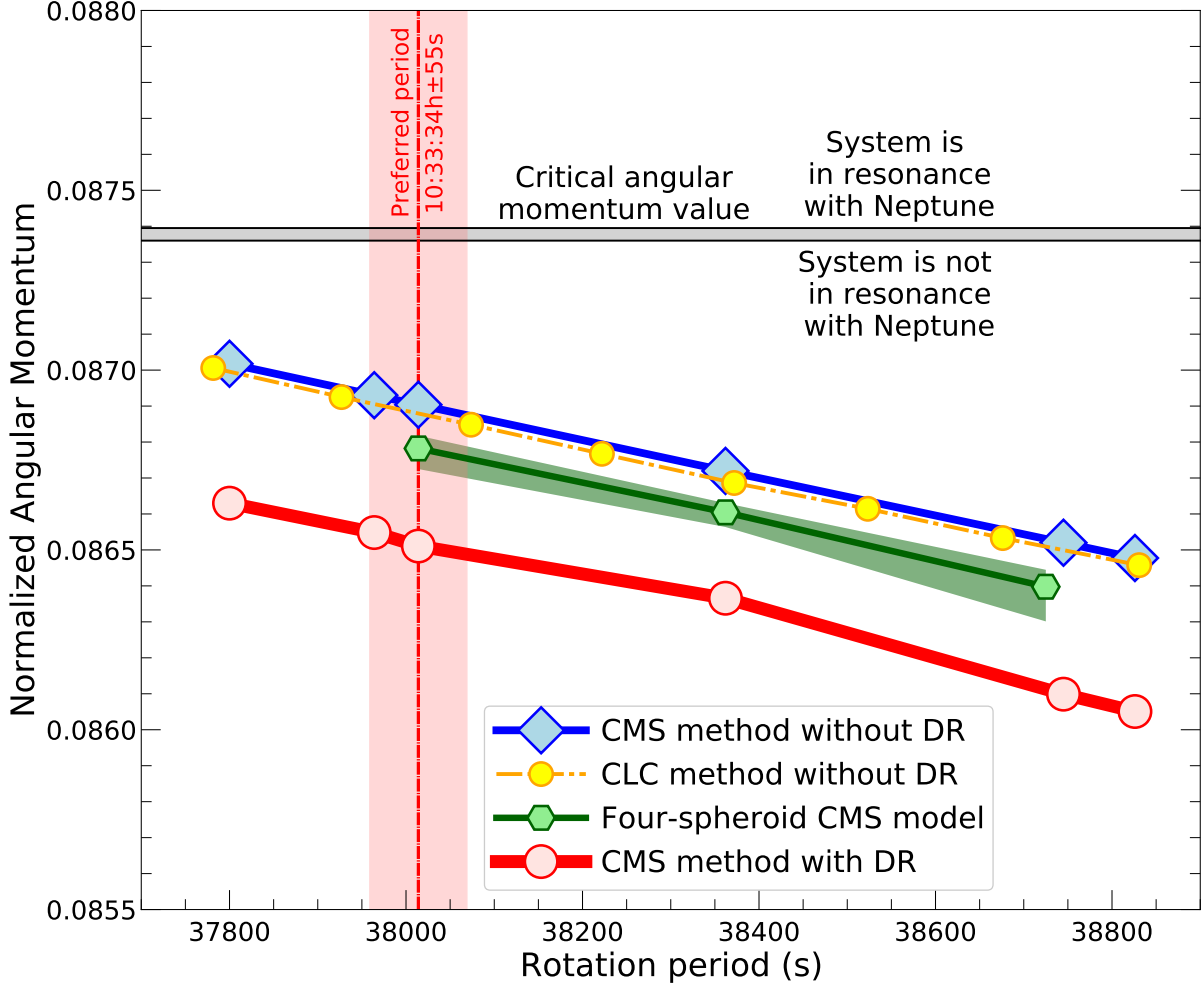


Figure 1: **Saturn's normalized angular momentum as a function of rotation period.** The red curve and circles represent results for models using physical equations of state with differential rotation, matched to the even gravitational moments up to J_{12} . The other three models assume uniform rotation and only match J_2 , J_4 , and J_6 . The results of the CLC method (yellow dash-dotted curve and small circles) and the CMS method (blue curve and diamonds) are consistent with each other, and close to the more approximate four spheroid CMS results (green curve and hexagons). The green shaded region indicates the range of results for an ensemble of four-spheroid CMS models that each match the gravitational moments. The vertical red line and band indicates the rotation period (and uncertainty) estimated from the measured flattening of Saturn. The horizontal grey band (between 0.087360 and 0.087399) indicates the critical value to be in the precession resonance. All models fall below the critical value, so the system is near, but not in, the spin-orbit precession resonance. Numeric values are listed in Table S1.

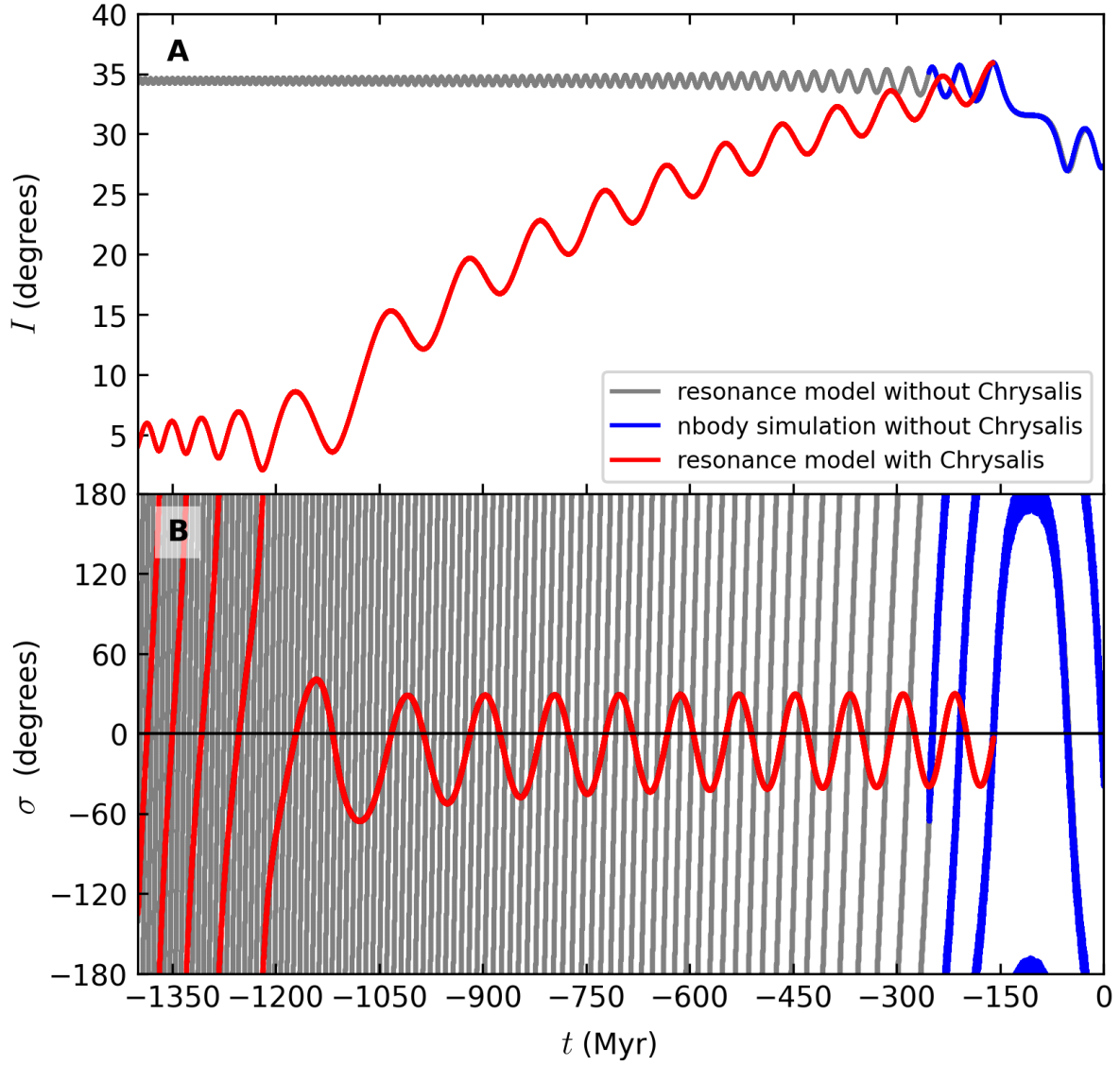


Figure 2: **Obliquity of Saturn I , and the resonance angle σ , as a function of time t .** The obliquity is with respect to the invariable plane, the plane perpendicular to the total angular momentum of the Solar System. The blue curve is a full numerical simulation, with $da_{\text{Titan}}/dt = 13.75 \text{ cm yr}^{-1}$, where a_{Titan} is the semimajor axis of Titan. The grey curve is the resonance model. At recent times it coincides with the blue curve. The red curve is the resonance model with Chrysalis. Chrysalis has an instability around 160 Myr before present and is removed from the system.

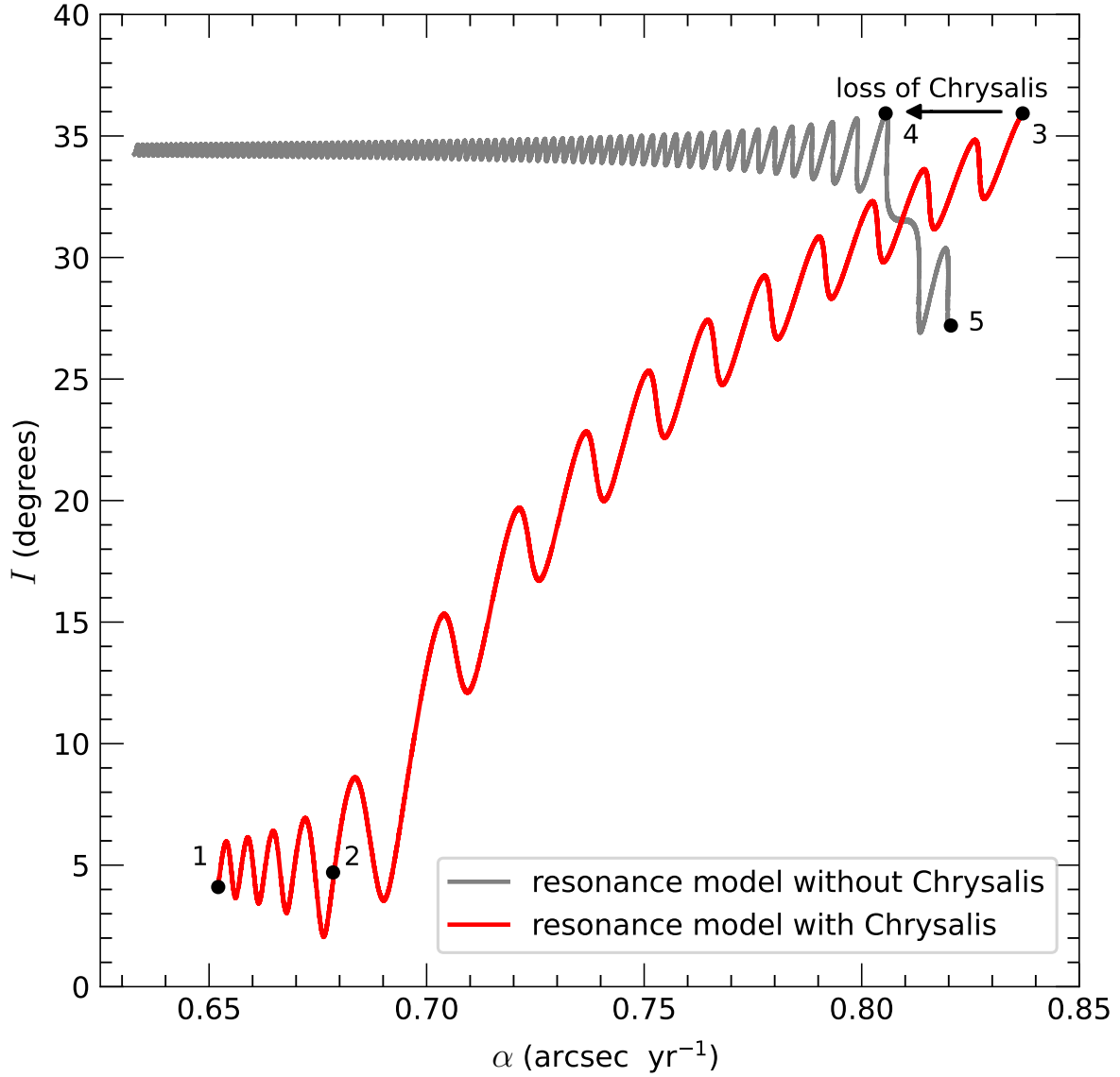


Figure 3: **Evolution as a function of precession constant.** The system starts outside the Neptune resonance at point 1. As Titan migrates, the precession constant increases, and the system enters the resonance at point 2. With continued evolution the obliquity of Saturn increases. At point 3 Chrysalis experiences an instability and has a close encounter with Saturn, forming the rings. The precession constant suddenly decreases to point 4. Further evolution, without Chrysalis, carries the system to point 5, at the present.

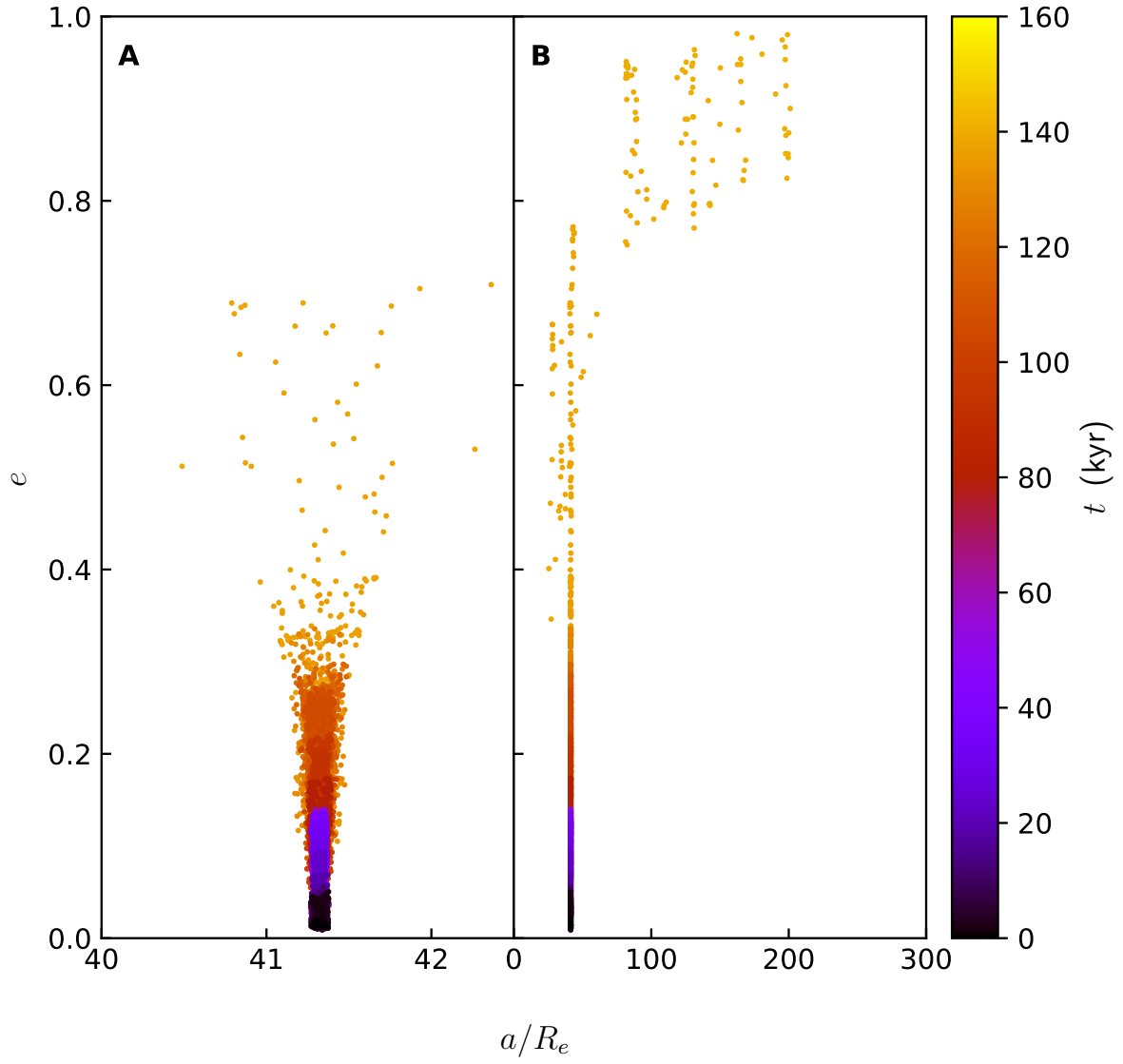


Figure 4: **Eccentricity of Chrysalis as a function of its semimajor axis, in an example simulation.** Time is indicated by the color bar. The early evolution in the chaotic zone is visible in panel A. In panel B, the chaotic phase shown in panel A appears as a spike on the left; the semimajor axis and eccentricity increase due to scattering encounters with Titan and Iapetus. The trajectory is sampled every 500 years.

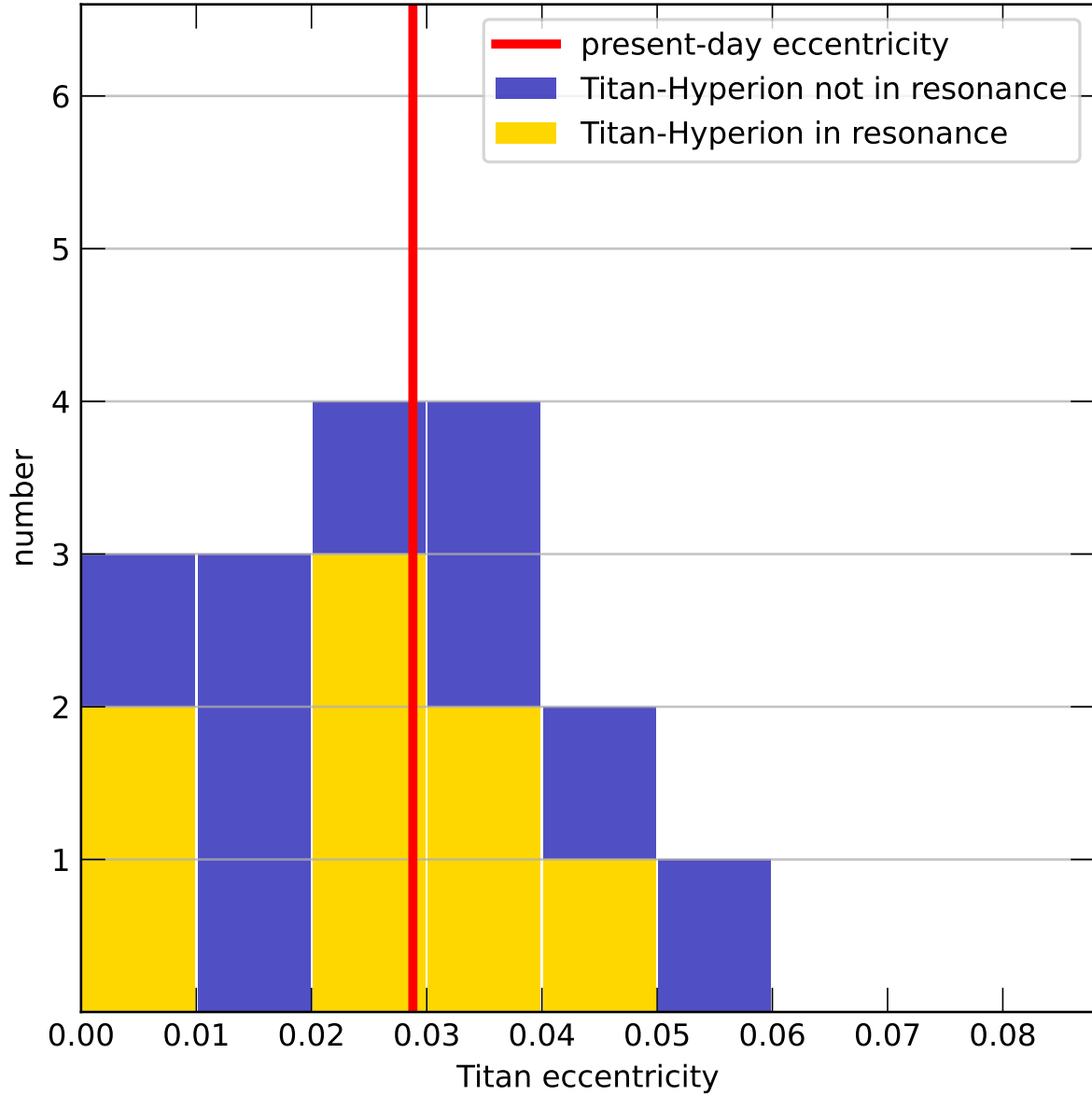


Figure 5: **Histogram of the eccentricity of Titan at the moment when Chrysalis experiences a grazing encounter with Saturn.** Yellow (blue) bars indicate simulations in which Titan and Hyperion are (are not) left in a 4:3 mean motion resonance, in which we find Hyperion today. The vertical red line indicates the current eccentricity of Titan.

Supplementary Materials for **The Origin of Saturn's Obliquity and Young Rings**

Jack Wisdom,* Rola Dbouk, Burkhard Militzer, William
B. Hubbard, Francis Nimmo, Brynna G. Downey, Richard
G. French

*Corresponding author. E-mail: wisdom@mit.edu.

This PDF file includes:

Materials and Methods

Supplementary Text

Figs. S1-S5

Table S1

References (34-51)

Materials and Methods

1. Numerical integration of satellite systems

We have investigated several aspects of this problem with full numerical integrations of the dynamical evolution of Saturn satellite system. These integrations include Saturn, modelled as a rigid body, the gravitational moments of Saturn from J_2 to J_6 , the major satellites of Saturn, from Mimas to Iapetus, the Sun, and the four outer planets. Initial conditions and parameters are taken from JPL ephemerides DE440 and SAT440 (34, 35).

We use the symplectic n-body mapping method (36) to evolve the orbits of the system, the axisymmetric Lie-Poisson method (37) to evolve the rigid body motion of Saturn, and the symplectic corrector (38) to remove integrator induced oscillations. We use a universal Kepler solver (39) that can handle hyperbolic orbits.

We use hierarchical Jacobi coordinates (40) to effect the splitting of the n-body Hamiltonian into Keplerian and interaction parts. The hierarchical Jacobi coordinates are useful here to describe the motion of the satellites, which orbit Saturn, which in turn orbits the Sun, and interacts with the other planets. The Jacobi coordinates allow the separation of the center of mass from the relative motions of the other bodies. Each Jacobi coordinate specifies the rectangular coordinates of a body relative to the center of mass of bodies higher in the tree. The Jacobi coordinates have the property that the kinetic energy is quadratic in the velocities, as is the kinetic energy in barycentric coordinates. This allows a splitting of the n -body Hamiltonian into Keplerian, interaction, and center of mass coordinates.

All gravitational interactions are included; the system is fully coupled. The gravitational moments affect the motion of the satellites as well as the rotation of Saturn. The oblateness of Saturn (J_2) interacting with the Sun affects Saturn's rotation (for example, inducing precession and nutation), as well as its orbit.

We use a stepsize that is ~ 15 times smaller than the shortest period being integrated (38).

For the Saturnian satellites, Mimas has the smallest orbit period of about 23 hours. For most of our integrations we adopt a stepsize of 0.06 days (or 1.44 hours).

We monitor the energy and angular momentum error of our integrations. For a 50 Myr integration, without tidal friction, the relative energy error of the whole system grows irregularly and is $\sim 5 \times 10^{-11}$. The relative error in the angular momentum is of order 2×10^{-10} .

The detailed precessional motion of Saturn’s spin axis due to Solar System and planetary torques was independently verified by comparison of numerical integration results with trigonometric series representations of the pole direction provided by JPL. We also took account of the uncertainty in the instantaneous direction of Saturn’s pole at the J2000 epoch, determined from Cassini observations of Saturn’s rings (41), when computing our suite of numerical integrations.

2. Resonance model We construct a simple model that captures many aspects of the dynamics of the secular spin-orbit resonance with Neptune. This model can be used to interpret the results of the full numerical simulations. For a varying orbit, the dynamics is described by the averaged time-dependent Hamiltonian (8, 10, 42).

$$H = -\frac{1}{2}C\omega\alpha(\cos\epsilon)^2/(1-e^2)^{3/2}, \quad (\text{S1})$$

where ϵ is the angle between the spin axis and the moving normal to the orbit, and e is Saturn’s orbital eccentricity. After expressing the Hamiltonian in terms of canonical coordinates that specify the orientation with respect to an inertial reference, the equations of motion are Hamilton’s equations (10, 42). The equations of motion are numerically integrated. We adopt the resonance locking expression for the evolution of the semimajor axis of Titan (14). The secular evolution of the orbit can be expressed as a sum of modes (43). Resonances occur if the precession frequency matches one of the mode frequencies.

A key feature of Eq. (2) is that the contribution from each satellite to q , the factor that is added to J_2 , is proportional to the product of the mass of the satellite and the square of

its distance from the planet. The contribution of Titan to the precession constant dominates the contribution from J_2 , and this contribution increases as Titan migrates outwards. Both Titan and Iapetus are sufficiently distant from Saturn that i^L is non-negligible. A Hamiltonian treatment that includes the precession constant as a parameter becomes inconsistent if there are distant satellites (13). Eq. (2) shows that the satellite contributions to the precession constant depend on the obliquity and the inclinations of the satellites to the Laplace plane. The obliquity varies, and so does the inclination to the Laplace plane, so actually the precession constant varies (13). This inconsistency is one reason why we have chosen to primarily investigate the evolution with full numerical integrations. Other investigations (12, 13) introduce additional approximations, for example, lumping all the other satellites into Titan. Nevertheless, the resonance model captures qualitative aspects of the dynamics.

3. Integration of unstable systems

Our integrations of the resonantly unstable systems require a smaller timestep, because there are close encounters. We can resolve an encounter by choosing a timestep that is near the orbital period of the satellite pair at a grazing distance, divided by 15. Applying this criterion to our systems, we have chosen a timestep of 0.0015 days (or 2.16 minutes). This is small, but the integrations of the unstable systems span less than 500 kyr. We find that with this stepsize, energy and angular momentum are conserved during encounters. The typical relative error in angular momentum at the end of these simulations is $\sim 10^{-11}$.

4. Tidal friction

If there is tidal friction, energy is no longer conserved but angular momentum is. For a given tidal model, we specify the rates da/dt , $(1/e)de/dt = \kappa_e$, and $(1/i)di/dt = \kappa_i$, where a , e , and i are the semimajor axis, eccentricity, and inclination to the equator of Titan's orbit, respectively, and κ_e and κ_i are the inverses of the timescales for eccentricity and inclination

damping. We additionally define $\kappa_a = (1/a)da/dt$.

Tidal friction is incorporated as velocity kicks. The magnitude of the kick is

$$\vec{k} = t_a \vec{v} + t_b \dot{r}(\hat{x} - (\dot{r}/v)\hat{v}) + t_g(\hat{p} \cdot \hat{v})(\hat{x} \times \vec{v}), \quad (\text{S2})$$

where \hat{x} is the direction of the relative vector \vec{x} , \hat{v} is the direction of the relative velocity \vec{v} , and \hat{p} is the direction of the pole of the planet. The constants are $t_a = \alpha_0 + e^2\alpha_1$, $t_b = \beta + 4e^2\alpha_1$, and $t_g = \gamma$, where e is the orbital eccentricity. Orbital inclinations damp to the Laplace plane. An angular momentum conserving kick is applied to the rotation. The constants α_0 , α_1 , β , and γ depend on the tidal model.

A rapid migration of Titan has been observed (14). This rapid migration is consistent with the resonance-locking theory of tidal evolution (44), in which the rate of evolution of oscillation modes in the planet controls the rate of satellite migration. For equilibrium tides, several terms in the tidal potential contribute to the evolution of the eccentricity (45). For resonance-locking tides, there is only a single term present, the 2200 term. In this case

$$\alpha_0 = \kappa_a/(2f) \quad (\text{S3})$$

$$\alpha_1 = (\kappa_e - (1/4)\kappa_a)/f \quad (\text{S4})$$

$$\beta = 2(\kappa_e - (1/4)\kappa_a) \quad (\text{S5})$$

$$\gamma = 2(\kappa_i - (1/4)\kappa_a) \quad (\text{S6})$$

where $f = a(2/r - 1/a)$, and r is the distance and a is the semimajor axis. These terms produce negligible evolution of the eccentricity and inclination, with a corresponding timescale of over 10 Gyr for Titan. For all practical purposes, the form for tidal friction that we adopt simply produces an evolution in semimajor axis.

For our tidally evolving simulations, we specify da/dt for Titan, but for simplicity ignore the tidal evolution of the other satellites. The measured rate of tidal evolution of Titan is 11 ± 2

cm yr⁻¹ (radio tracking) and 25.3 ± 20.9 cm yr⁻¹ (astrometry) (14); we explored the rates 7.33 cm yr⁻¹, 10.00 cm yr⁻¹, 12.22 cm yr⁻¹, 13.75 cm yr⁻¹, 15.71 cm yr⁻¹, and 22.00 cm yr⁻¹.

We also ignored eccentricity and inclination damping due to satellite tides. In some of our simulations Titan eccentricities and inclinations are larger than their present-day values. We expect modest damping of both e and i to occur due to satellite tides over the ~ 150 Myr following excitation. Eccentricity damping depends on Titan's k_2/Q ; the measured potential Love number k_2 is approximately 0.6, but only a lower bound on the dissipation parameter Q is available (46). A Q of ~ 60 would be sufficient to damp Titan's eccentricity by a factor of two over 150 Myr. Inclination damping is probably dominated by obliquity tides in the subsurface ocean; the resulting damping timescale is ~ 300 Myr (47), short enough that some damping should have occurred.

Supplementary Text

1. Models of Saturn Interior and Angular Momentum Constraints

Here we present results from additional interior models. Our analysis relies on the result that high-precision spacecraft measurements of Saturn’s gravity harmonics J_2 , J_4 , and J_6 constrain the planet’s normalized angular momentum \mathcal{J} sufficiently tightly to exclude values at or above the critical value for resonance with Neptune, \mathcal{J}_c , where we find that \mathcal{J}_c lies in the small range $0.087360 - 0.087395$. Some values of \mathcal{J} permitted by the gravity harmonics lie as close as 0.5% below \mathcal{J}_c , but here we verify that modeling uncertainties do not eliminate this gap. Saturn’s axial precession is currently not in resonance with Neptune.

The published J_2 , J_4 , and J_6 are normalized to $R_e = 60330$ km, whereas our interior models are matched to values normalized to the observed 1-bar radius, $R_e = 60268$ km. All normalizations in our calculations are consistent with the latter number.

In Fig. S2, we plot the probability density of permitted angular momentum values that result from ensembles of models with four constant-density spheroids that a) match only J_2 , b) match J_2 and J_4 , or c) match J_2 , J_4 , as well as J_6 . If only J_2 is matched, angular momentum values above the critical value are permitted. Already if J_4 is added to constrain the models, angular momentum values near or above the critical value are excluded. If J_6 is introduced as a model constraint, lower angular momentum values are excluded also. All these calculations were performed with the CMS method using four spheroids. The equatorial radii and the density of the three inner spheroids were allowed to vary. The shapes of the spheroids were adjusted until they represented equipotential surfaces. Then the gravity harmonics and angular momentum were derived. No effects from differential rotation were included. In Fig. S2, we report results of a single rotation period of 10:33:34 h while Fig. 1 shows results over a range of periods.

In Fig. S3, we show the probability density of angular momentum from CMS calculations with 6, 8, 10, 15, and 20 spheroids. We find that increasing the number of spheroids does not

enable us to construct models that yield larger angular momenta while matching the observed gravity harmonics J_2 , J_4 , and J_6 . To reduce the parameter space, we constrained the equatorial spheroid radii to reside on the linear grid in radius rather than allowing them to be varied as we did in our four-spheroid models in Fig. S2.

In Fig. S4, we show the probability density of angular momentum for models matching four different J_6 values while matching the measured values of J_2 and J_4 . The figure shows that an assumed decrease in J_6 corresponds to a decrease in the likely angular momentum, and larger changes in J_6 correspond to larger changes in the likely angular momentum. We find that the models without differential rotation in Fig. 1 represent an upper bound to the inferred angular momentum. Every model ensemble includes assumptions and approximations. But if, for a given set of assumptions, differential rotation is introduced to an ensemble, the inferred angular momentum is reduced. This shifts the angular momentum farther away from the critical value, which again supports our conclusion that Saturn is not in resonance with Neptune today. This argument rests on the following points:

1. Fig. 1 shows that models with differential rotation predict smaller angular momenta than models that match J_2 , J_4 , and J_6 without it.
2. Fig. S1 shows that the effects of differential rotation increase the higher-order gravity harmonics. The increase of J_6 is approximately 6×10^{-6} .
3. In our Saturn models that include differential rotation, most of the contribution to J_6 comes from the interior but there is also a positive contribution from the differential rotation. The latter term reduces the contribution to J_6 from the interior to below the equivalent value from a model without differential rotation, in which the entire J_6 contribution comes from the interior.
4. A reduced contribution to J_6 from the interior leads to a reduction of the angular momen-

tum as we show in Fig. S4. Therefore models invoking differential rotation to contribute a fraction to J_6 , predict smaller angular momenta than models without differential rotation, which yield an upper bound to the inferred angular momentum. This is consistent with the results in Fig. 1.

2. Orbital resonances encountered

As the system is evolved backwards in time, two principal orbital resonances are encountered, which have been previously studied: the 5:1 mean motion Titan-Iapetus resonance (in which the orbital period of Iapetus is approximately five times the orbital period of Titan) (48), and a complicated secular resonance involving the orbit of Iapetus, the longitude of the equator of Saturn, and the longitude of the perihelion of Jupiter (26). The resonant argument of this secular resonance is $\varpi - \varpi_J + \Omega - \Omega_{\text{eq}}$, where ϖ and Ω are the longitudes of the pericenter and ascending node of Iapetus, ϖ_J is the longitude of the pericenter of Jupiter, and Ω_{eq} is the longitude of the equator of Saturn. Another orbital resonance that affects the backward evolutions is the 7:2 mean motion Rhea-Titan resonance, with resonant argument $7\lambda_T - 2\lambda_R - \varpi_R - 4\varpi_T$, where λ_T and λ_R are the mean longitudes of Titan and Rhea, respectively, and ϖ_T and ϖ_R are the longitudes of their pericenters.

None of these resonances affects the precession constant enough for the system to leave the Neptune spin-orbit precession resonance.

3. Disruption Radius

The outer edge of the A-ring, the outermost of Saturn's main rings, is around $2.3R_e$; for a density of 1 g cm^{-3} the distance from the planet at which a body without strength or viscosity is pulled apart is around $2.1R_e$ (49). The distance below which disruption occurs is uncertain. Bodies with finite viscosity (50) or internal shear strength (51) may experience disruption at somewhat smaller distances.

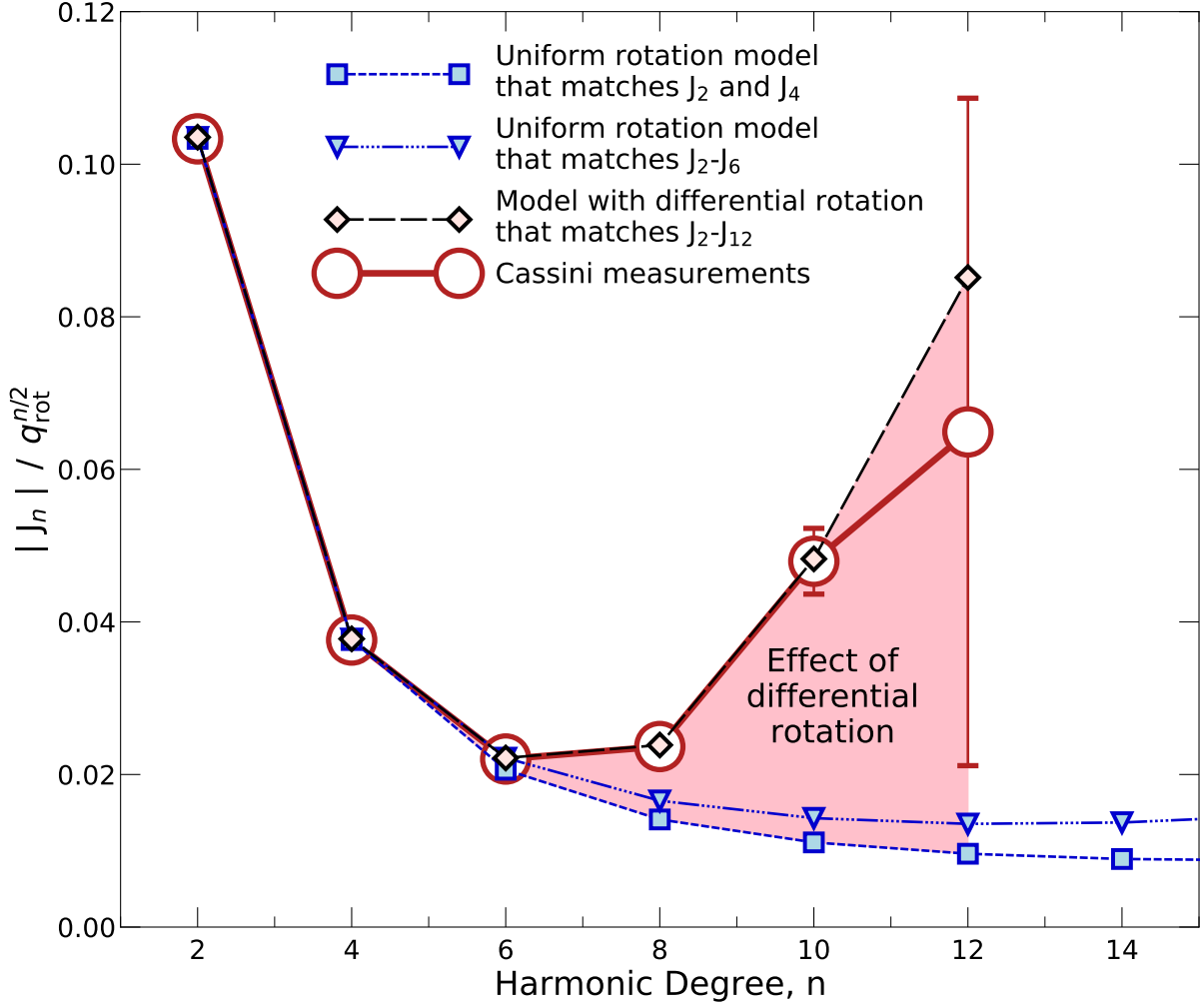


Figure S1: **The gravitational moments, J_n , versus degree.** The interior models with differential rotation fit the observed moments up to J_{12} within their errors. All moments have been scaled by powers of the rotational parameter $q_{\text{rot}} = \omega^2 R_e^3 / GM$. See (18). Moments of a model that match J_2 and J_4 with uniform rotation (blue dashed curve with blue boxes), a model that matches J_2 , J_4 , and J_6 with uniform rotation (blue dot-dashed curve with blue triangles), a model that matches $J_2 - J_{12}$ with differential rotation (dashed black line with yellow diamonds), with Cassini measurements and errors (red curve with red circles). The effect of differential rotation is shaded light red.

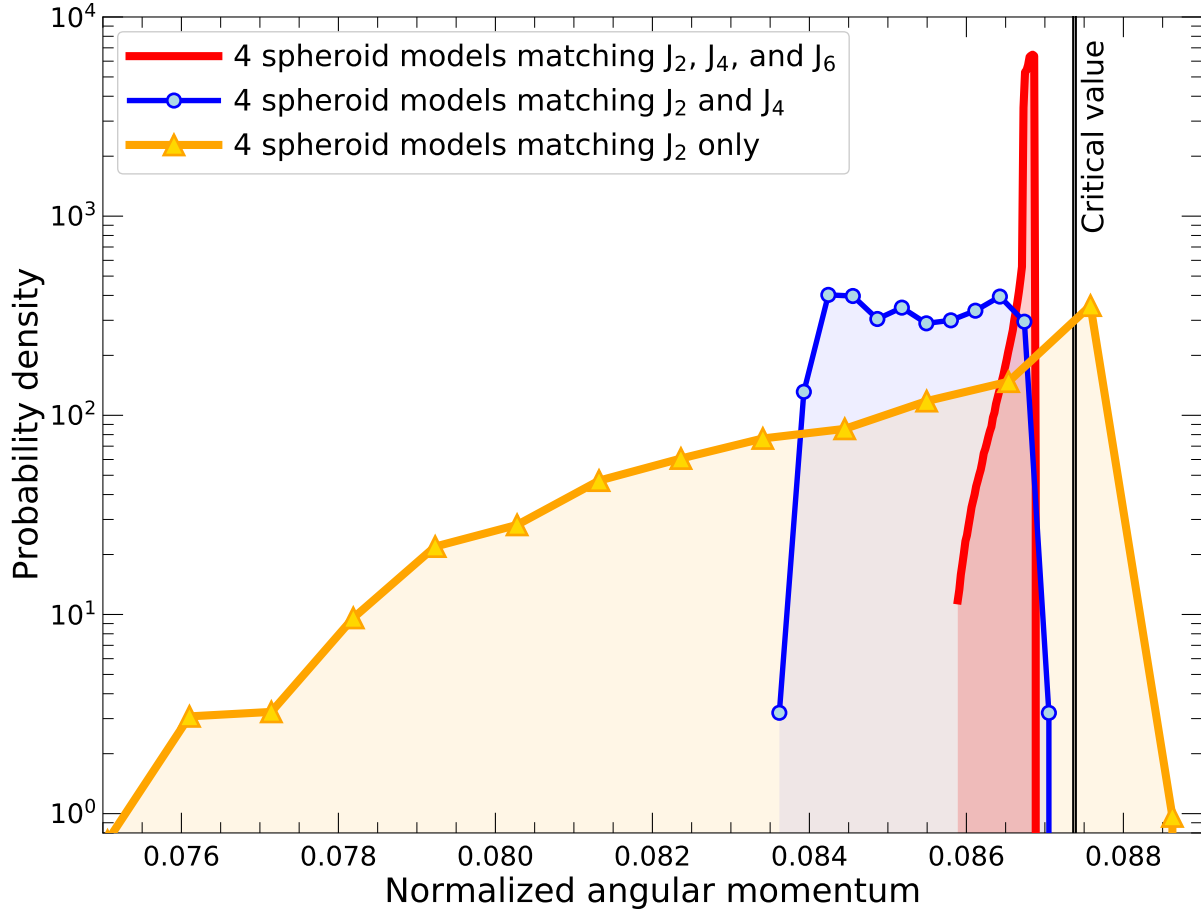


Figure S2: **Probability density of model predictions for the normalized angular momentum.** Ensembles of models that match the gravity harmonic J_2 only (orange curve and orange triangles), match J_2 and J_4 (blue curve and blue circles), or match all three harmonics J_2 , J_4 , and J_6 (red curve). Only with models that solely match J_2 is it possible to obtain angular momentum values around or above the critical value (grey band between the vertical black lines). J_2 and J_4 together constrain the moment of inertia sufficiently well to exclude values near the critical value. J_6 narrows the range of permitted angular momentum values further by excluding low values. All calculations were performed for a rotation period of 10:33:34 h with the CMS method using four spheroids.

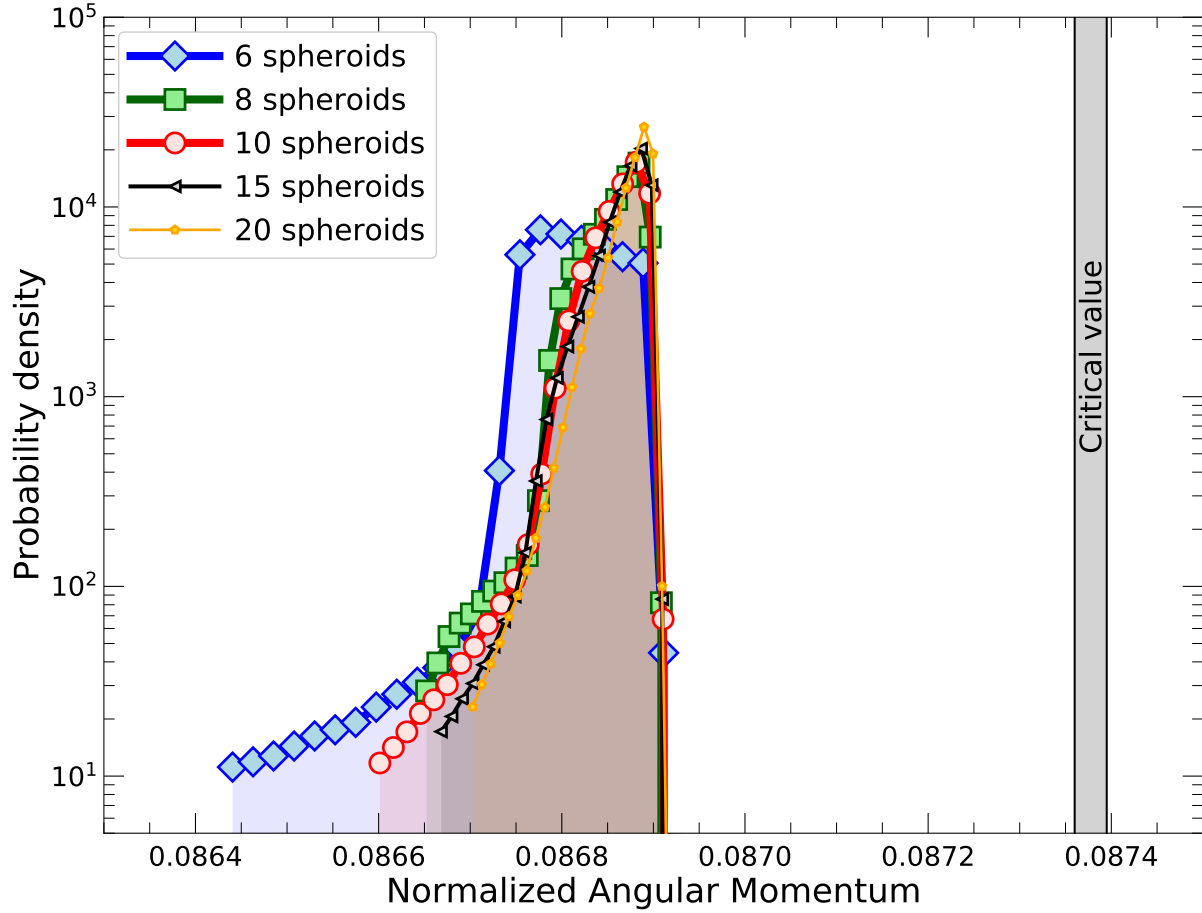


Figure S3: **Probability density of model predictions for the normalized angular momentum.** Ensembles of models with 6 spheroids (blue curve with blue diamonds), 8 spheroids (green curve with green squares), 10 spheroids (red curve with red circles), 15 spheroids (black curve with black triangles), and 20 spheroids (orange curve with orange dots) that match the observed gravity harmonics J_2 , J_4 , and J_6 . The diagram shows that adding additional spheroids to the models does not enable one to approach the critical angular momentum value (vertical grey band). All calculations were performed with the CMS method without differential rotation for a rotation period of 10:33:34 h.

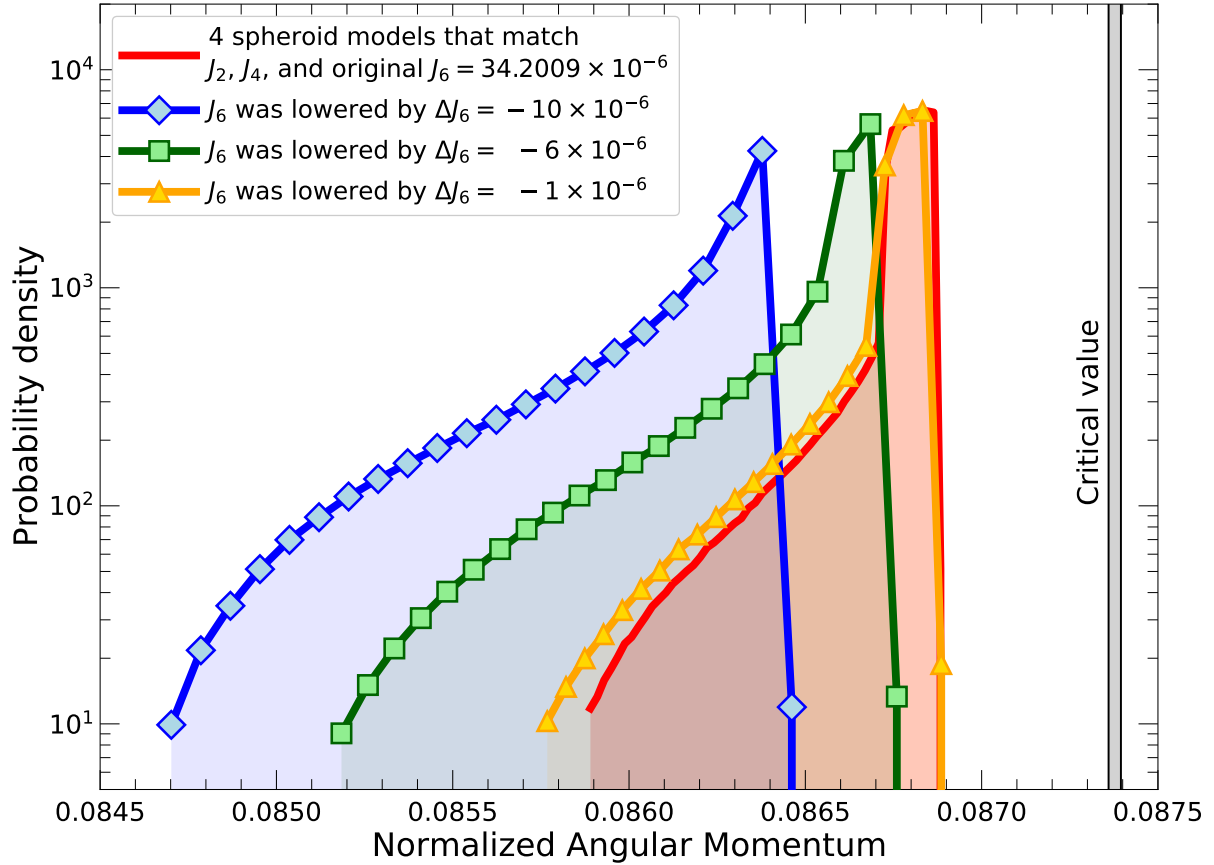


Figure S4: **Probability density of model predictions for the normalized angular momentum.** Ensembles of models that match the observed gravity harmonics J_2 , J_4 , and four different values of J_6 (original (red curve), lowered by -1×10^{-6} (orange curve and orange triangles), lowered by -6×10^{-6} (green curve with green boxes), lowered by -10×10^{-6} (blue curve with blue diamonds)). There is a correlation between the J_6 value and the inferred angular momentum. All calculations were performed without differential rotation for a rotation period of 10:33:34 h with the CMS method using four spheroids.

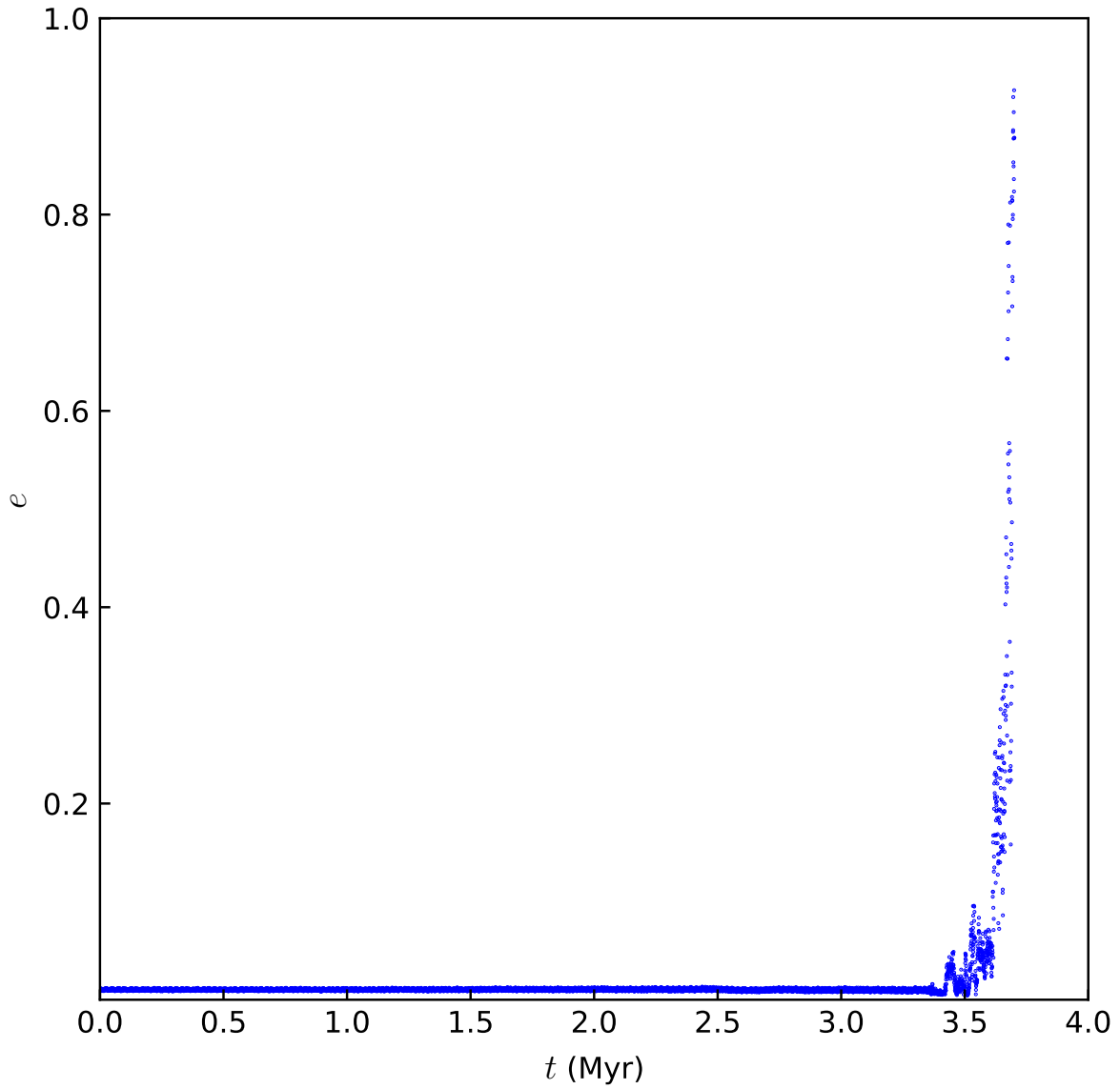


Figure S5: **Eccentricity of Chrysalis as a function of time.** A simulation in which the system encounters the 3:1 Titan-Chrysalis resonance as Titan tidally migrated outwards. The orbit of Chrysalis becomes chaotic and the eccentricity rapidly becomes large enough for encounters with the other satellites. This simulation included Hyperion.

Table S1: Values of Saturn's normalized angular momentum of Saturn in Fig. 1.

Method	Rotation Period (s)	Normalized Angular Momentum
CMS method with DR	37800	0.08662998
	37964	0.08654830
	38014	0.08651077
	38362	0.08636567
	38745	0.08609887
	38826	0.08605070
CMS method without DR	37800	0.08701761
	37964	0.08693018
	38014	0.08690372
	38362	0.08671972
	38745	0.08652001
	38826	0.08647747
CLC method without DR	37782	0.08700588
	37927	0.08692498
	38074	0.08684816
	38222	0.08676730
	38372	0.08668612
	38523	0.08661436
	38676	0.08653295
	38831	0.08645762
Four-spheroid CMS model without DR	38014	0.08678220
	38362	0.08660454
	38725	0.08639766